INTERNATIONAL JOURNAL FOR NUMERICAL METHODS IN FLUIDS, VOL. 27, 109–125 (1998)

CAVITATION MODELLING IN SATURATED GEOMATERIALS WITH APPLICATION TO DYNAMIC STRAIN LOCALIZATION

D. GAWIN[1]* L. SANAVIA[2] AND B. A. SCHREFLER[2]

[1]*Department of Building Physics and Building Materials, Technical University of Lodz, Al. Politechniki 6, 93–590 Lodz, Poland*
[2]*Istituto di Scienza e Tecnica delle Construzioni, Università di Padova, Via Marzolo 9, I-35131, Padova, Italy*

SUMMARY

A model to simulate cavitation phenomena in the pores of saturated porous media is developed. Such phenomena appear in connection with pore water traction, which may be observed during strain localization in dense sand samples or in dynamic fluid–structure interaction problems where the structure is made of geomaterials. The model makes use of an isothermal two-phase flow approach. Numerical examples relating to strain localization are shown. © 1998 John Wiley & Sons, Ltd.

Int. J. Numer. Meth. Fluids, **27**: 109–125 (1998)

KEY WORDS: multiphase porous material; cavitation; water pressure; vapour pressure; strain localization; finite element method

1. INTRODUCTION

Cavitation, which means the nucleation of the phase change to vapour, occurring when the absolute pressure of water decreases below the vapour saturation pressure, is not too common in geomaterials. However, it sometimes plays an important role. For instance, cavitation has been observed in strain localization experiments carried out on undrained samples of dense sand[1] and it has been stated that in such situations localization starts only if cavitation takes place. Cavitation has also been observed numerically in fluid–structure interaction problems, e.g. at the interface between a concrete dam and the water of the reservoir if they are subject to seismic excitation.[2]

A simplified approach to the modelling of cavitation in dynamic situations was presented in Reference 3, where the mass balance equation of vapour was neglected as well as the energy balance equation. This may be considered as an isothermal monospecies approach, but was found useful in strain localization models to follow the shear band from its onset up to its full development. In this paper we develop a more complete isothermal two-phase flow model where phase change and the mass balance equation of vapour are taken into account.

*Correspondence to: D. Gawin, Department of Building Physics and Building Materials, Technical University of Lodz, Al. Politechniki 6, 93-590 Lodz, Poland.

Contract grant sponsor: Italian Ministry of Scientific and Technological Research; Contract grant number: MURST 40%.

CCC 0271–2091/98/010109–17 $17.50 *Received May 1996*
© 1998 John Wiley & Sons, Ltd.

We first present briefly the full model for non-isothermal behaviour of partially saturated deforming porous media, from which our applied model stems. Then we discuss the introduced simplifications and the numerical solution of the resulting equations. These solutions are obtained with a modified version of the Swandyne code.[4,5]

Finally we show applications of this model to the dynamic strain localization problem and compare the results with those of the previous simplified approach.

2. GENERAL MATHEMATICAL MODEL OF THERMOHYDROMECHANICAL TRANSIENT BEHAVIOUR OF GEOMATERIALS

The full mathematical model necessary to simulate thermohydromechanical transient behaviour of fully and partially saturated porous media was developed in Reference 6 using averaging theories following Hassanizadeh and Gray.[7–9] Based on it, the general cavitation model and its simplified version (monospecies approach) were presented in Reference 3.

The underlying physical model, thermodynamic relations and constitutive equations as well as governing equations are briefly summarized here for the sake of completeness.

The partially saturated porous medium is treated as a multiphase system with the voids of the solid skeleton filled partly with liquid and partly with gas. The latter is assumed to behave as an ideal mixture of two species: dry air (non-condensable gas) and water vapour (condensable gas). The state of the medium is described by the water pressure p^{w}, the gas pressure p^{g}, the temperature T and the displacement vector of the solid matrix, $\mathbf{u}$. Small displacements are assumed for the development of the equations. Local thermal equilibrium between solid matrix, gas and liquid phases is assumed, so the temperature is the same for all the constituents.

The saturation of liquid water, S_{w}, is an experimentally determined function of the capillary pressure p^{c} and the temperature T, i.e.

$$S_{\mathrm{w}} = S_{\mathrm{w}}(p^{\mathrm{c}}, T), \tag{1}$$

while the capillary pressure p^{c} can be expressed at equilibrium[10] as

$$p^{\mathrm{c}} = p^{\mathrm{g}} - p^{\mathrm{w}}, \tag{2}$$

where p^{g} is the pressure of the dry air and water vapour mixture.

The equation of state of a perfect gas (the Clapeyron equation) and Dalton's law applied to dry air (ga), water vapour (gw) and moist air (g) yield

$$p^{\mathrm{ga}} = \rho^{\mathrm{ga}} RT/M_{\mathrm{a}}, \qquad p^{\mathrm{gw}} = \rho^{\mathrm{gw}} RT/M_{\mathrm{w}}, \tag{3}$$

$$p^{\mathrm{g}} = p^{\mathrm{ga}} + p^{\mathrm{gw}}, \qquad \rho^{\mathrm{g}} = \rho^{\mathrm{ga}} + \rho^{\mathrm{gw}}. \tag{4}$$

Owing to the curvature of the meniscus separating the liquid (water) phase from the gas phase inside the pores of the medium (considered as a capillary porous body), the equilibrium water vapour pressure p^{gw} differs from the saturation pressure p^{gws} and can be obtained from the Kelvin equation

$$p^{\mathrm{gw}} = p^{\mathrm{gws}}(T) \exp\left(-\frac{p^{\mathrm{c}} M_{\mathrm{w}}}{\rho^{\mathrm{w}} RT}\right), \tag{5}$$

where the water vapour saturation pressure p^{gws}, depending only on the temperature T, can be calculated from the Clausius–Clapeyron equation or from empirical correlations (see e.g. Reference 11).

 © 1998 John Wiley & Sons, Ltd.

The constitutive law for the solid phase is introduced through the concept of the modified effective stress

$$\boldsymbol{\sigma}'' = \boldsymbol{\sigma} + \bar{\alpha} p \mathbf{I}, \tag{6}$$

where $\boldsymbol{\sigma}''$ is the total Cauchy stress tensor, $\mathbf{I}$ is the unit second-order tensor, $\bar{\alpha}$ is Biot's constant and p is the average pressure of the mixture of fluids surrounding the grains, which in the case of a small dependence of Helmholtz free energies on void fraction is given[10] by the commonly employed relation

$$p = S_{\mathrm{w}} p^{\mathrm{w}} + S_{\mathrm{g}} p^{\mathrm{g}} - p_{\mathrm{atm}}, \tag{7}$$

where $S_{\mathrm{w}} + S_{\mathrm{g}} = 1$. The last term in (7) has been added because we use absolute pressures here, and pure atmospheric pressure does not cause any deformation of the medium.

The constitutive relationship for the solid skeleton has the form

$$\mathrm{d}\boldsymbol{\sigma}'' = \mathbf{C}_{\mathrm{T}}(\mathrm{d}\varepsilon - \mathrm{d}\varepsilon^{\mathrm{T}} - \mathrm{d}\varepsilon^{\mathrm{o}}), \tag{8}$$

where $\mathbf{C}_{\mathrm{T}}$ is the tangent constitutive tensor, $\mathrm{d}\varepsilon^{\mathrm{T}} = \mathbf{I}(\beta_{\mathrm{s}}/3)\,\mathrm{d}T$ is the strain increment caused by thermoelastic expansion, with β_{s} the cubic thermal expansion coefficient of the solid, and $\mathrm{d}\varepsilon^{\mathrm{o}}$ represents the autogeneous strain increments and the irreversible part of the thermal strain tensor.[12]

For the binary gas mixture of dry air and water vapour, Fick's law gives the following relative average velocities $\mathbf{v}_{\mathrm{g}}^{\pi}$ of the diffusing species:[13]

$$\mathbf{v}_{\mathrm{g}}^{\mathrm{ga}} = -\frac{M_{\mathrm{a}} M_{\mathrm{w}}}{M_{\mathrm{g}}^2} \mathbf{D}_{\mathrm{g}} \operatorname{grad}\left(\frac{p^{\mathrm{ga}}}{p^{\mathrm{g}}}\right) = \frac{M_{\mathrm{a}} M_{\mathrm{w}}}{M_{\mathrm{g}}^2} \mathbf{D}_{\mathrm{g}} \operatorname{grad}\left(\frac{p^{\mathrm{gw}}}{p^{\mathrm{g}}}\right) = -\mathbf{v}_{\mathrm{g}}^{\mathrm{gw}}, \tag{9}$$

where

$$\frac{1}{M_{\mathrm{g}}} = \frac{\rho^{\mathrm{gw}}}{\rho^{\mathrm{g}}} \frac{1}{M_{\mathrm{w}}} + \frac{\rho^{\mathrm{ga}}}{\rho^{\mathrm{g}}} \frac{1}{M_{\mathrm{a}}}. \tag{10}$$

In (9), $\mathbf{D}_{\mathrm{g}}$ is the effective diffusivity tensor and M_{g} is the molar mass of the gas mixture.

The linear momentum balance equation for the fluids, after neglecting several terms of minor importance,[12,14,15] can be written in the form of the generalized Darcy equation

$$\mathbf{v}^{\pi \mathrm{s}} = \frac{\mathbf{k} k^{r\pi}}{\mu^{\pi}} [-\operatorname{grad} p^{\pi} + \rho^{\pi}(\mathbf{g} - \mathbf{a}^{\mathrm{s}} - \mathbf{a}^{\pi \mathrm{s}})], \tag{11}$$

where $\pi = \mathrm{w}$ or g, $\mathbf{v}^{\pi \mathrm{s}}$ is the intrinsic mass-averaged velocity relative to the solid, $\mathbf{a}^{\pi \mathrm{s}}$ is the acceleration relative to the solid and the term $\mathbf{k} k^{r\pi}/\mu^{\pi}$ expresses the fluid–solid exchange of momentum. The relative permeability $k^{r\pi}$ is a function of the degree of saturation S_{π} and the temperature T, $\mathbf{k}$ is the intrinsic permeability tensor and μ is the dynamic viscosity.

The linear momentum balance equation for the multiphase medium has the form[6]

$$\operatorname{div} \boldsymbol{\sigma} + \rho(\mathbf{g} - \mathbf{a}^{\mathrm{s}}) - n S_{\mathrm{w}} \rho^{\mathrm{w}} \mathbf{a}^{\mathrm{ws}} - n S_{\mathrm{g}} \rho^{\mathrm{g}} \mathbf{a}^{\mathrm{gs}} = 0, \tag{12}$$

where ρ is the average density of the multiphase medium given by

$$\rho = (1 - n)\rho^{\mathrm{s}} + \sum_{\pi \neq \mathrm{s}} n S_{\pi} \rho^{\pi}. \tag{13}$$

The dry air mass balance equation, after application of Darcy's law and Fick's law and neglecting acceleration terms, is

$$\frac{\partial}{\partial t}(n S_{\mathrm{g}} \rho^{\mathrm{ga}}) + S_{\mathrm{g}} \rho^{\mathrm{ga}} \operatorname{div} \mathbf{v}^{\mathrm{s}} - \operatorname{div}\left(\rho^{\mathrm{ga}} \frac{\mathbf{k} k^{\mathrm{rg}}}{\mu^{\mathrm{g}}} \operatorname{grad} p^{\mathrm{g}}\right) + \operatorname{div}\left[\rho^{\mathrm{g}} \frac{M_{\mathrm{a}} M_{\mathrm{w}}}{M^2} \mathbf{D}_{\mathrm{g}} \operatorname{grad}\left(\frac{p^{\mathrm{gw}}}{p^{\mathrm{g}}}\right)\right] = 0. \tag{14}$$

© 1998 John Wiley & Sons, Ltd.

The water vapour mass balance and liquid water mass balance equations are summed to eliminate the source term related to phase change, yielding the mass balance equation for all water species. After introduction of Darcy's law and Fick's law, as above, we obtain

$$\frac{\partial}{\partial t}(nS_{\mathrm{g}}\rho^{\mathrm{gw}}) + S_{\mathrm{g}}\rho^{\mathrm{gw}}\,\mathrm{div}\,\mathbf{v}^{\mathrm{s}} - \mathrm{div}\left(\rho^{\mathrm{gw}}\frac{\mathbf{k}k^{\mathrm{rg}}}{\mu^{\mathrm{g}}}\mathrm{grad}\,p^{\mathrm{g}}\right) - \mathrm{div}\left[\rho^{\mathrm{g}}\frac{M_{\mathrm{a}}M_{\mathrm{w}}}{M^2}\mathbf{D}_{\mathrm{g}}\,\mathrm{grad}\left(\frac{p^{\mathrm{gw}}}{p^{\mathrm{g}}}\right)\right]$$
$$= -\frac{\partial}{\partial t}(nS_{\mathrm{w}}\rho^{\mathrm{w}}) - S_{\mathrm{w}}\rho^{\mathrm{w}}\,\mathrm{div}\,\mathbf{v}^{\mathrm{s}} + \mathrm{div}\left(\rho^{\mathrm{w}}\frac{\mathbf{k}k^{\mathrm{rw}}}{\mu^{\mathrm{w}}}[\mathrm{grad}\,p^{\mathrm{w}} - \rho^{\mathrm{w}}(\mathbf{g} - \mathbf{a}^{\mathrm{s}} - \mathbf{a}^{\mathrm{ws}})]\right). \tag{15}$$

The macroscopic mass balance equation for the solid has already been summed with the above mass balance equations (14) and (15) to eliminate the time derivative of porosity n.

The energy conservation equation (enthalpy balance) can be expressed in the form[6]

$$\rho C_{\mathrm{p}}\frac{\partial T}{\partial t} - \mathrm{div}(\lambda_{\mathrm{eff}}\,\mathrm{grad}\,T) - \left(C_{\mathrm{p}}^{\mathrm{w}}\rho^{\mathrm{w}}\frac{\mathbf{k}k^{\mathrm{rw}}}{\mu^{\mathrm{w}}}[\mathrm{grad}\,p^{\mathrm{w}} - \rho^{\mathrm{w}}(\mathbf{g} - \mathbf{a}^{\mathrm{s}} - \mathbf{a}^{\mathrm{ws}})] + C_{\mathrm{p}}^{\mathrm{g}}\rho^{\mathrm{g}}\frac{\mathbf{k}k^{\mathrm{rg}}}{\mu^{\mathrm{g}}}\mathrm{grad}\,p^{\mathrm{g}}\right)\mathrm{grad}\,T$$
$$= \Delta h_{\mathrm{vap}}\left[\frac{\partial}{\partial t}(nS_{\mathrm{w}}\rho^{\mathrm{w}}) + S_{\mathrm{w}}\rho^{\mathrm{w}}\,\mathrm{div}\,\mathbf{v}^{\mathrm{s}} - \mathrm{div}\left(\rho^{\mathrm{w}}\frac{\mathbf{k}k^{\mathrm{rw}}}{\mu^{\mathrm{w}}}[\mathrm{grad}\,p^{\mathrm{w}} - \rho^{\mathrm{w}}(\mathbf{g} - \mathbf{a}^{\mathrm{s}} - \mathbf{a}^{\mathrm{ws}})]\right)\right], \tag{16}$$

where

$$\rho C_{\mathrm{p}} = nS_{\mathrm{w}}\rho^{\mathrm{w}}C_{\mathrm{p}}^{\mathrm{w}} + nS_{\mathrm{g}}\rho^{\mathrm{g}}C_{\mathrm{p}}^{\mathrm{g}} + (1-n)\rho^{\mathrm{s}}C^{\mathrm{s}} \tag{17}$$

is the heat capacity of the multiphase medium at constant pressure, λ_{eff} is the effective thermal conductivity of the moist material and Δh_{vap} is the latent heat of evaporation.

For model closure it is necessary to define the initial and boundary conditions.

The initial conditions specify the full fields of gas pressure, water pressure, temperature and displacements:

$$p^{\mathrm{g}} = p_{\mathrm{o}}^{\mathrm{g}}, \quad p^{\mathrm{w}} = p_{\mathrm{o}}^{\mathrm{w}}, \quad T = T_{\mathrm{o}}, \quad \mathbf{u} = \mathbf{u}_{\mathrm{o}} \quad \text{at } t = t_{\mathrm{o}}. \tag{18}$$

The boundary conditions can be imposed values on Γ_π or fluxes on Γ_π^{q}, where the boundary is $\Gamma = \Gamma_\pi \cup \Gamma_\pi^{\mathrm{q}}$. The imposed values on the boundary for gas pressure, water pressure, temperature and displacements are

$$p^{\mathrm{g}} = \hat{p}^{\mathrm{g}} \quad \text{on } \Gamma_{\mathrm{g}}, \quad p^{\mathrm{w}} = \hat{p}^{\mathrm{w}} \quad \text{on } \Gamma_{\mathrm{w}}, \quad T = \hat{T} \quad \text{on } \Gamma_{\mathrm{T}}, \quad \mathbf{u} = \hat{\mathbf{u}} \quad \text{on } \Gamma_{\mathrm{u}} \quad \text{for } t \geqslant t_{\mathrm{o}}, \tag{19}$$

The volume-averaged flux boundary conditions for the water species and dry air conservation equations and the energy equation to be imposed at the interface between the porous medium and the surrounding fluid (the natural boundary conditions) are

$$(\rho^{\mathrm{ga}}\mathbf{v}^{\mathrm{g}} - \rho^{\mathrm{g}}\mathbf{v}_{\mathrm{g}}^{\mathrm{gw}})\mathbf{n} = q^{\mathrm{ga}} \quad \text{on } \Gamma_{\mathrm{g}}^{\mathrm{q}}, \tag{20a}$$

$$(\rho^{\mathrm{gw}}\mathbf{v}^{\mathrm{g}} + \rho^{\mathrm{w}}\mathbf{v}^{\mathrm{w}} + \rho^{\mathrm{g}}\mathbf{v}_{\mathrm{g}}^{\mathrm{gw}})\mathbf{n} = \beta_{\mathrm{c}}(\rho^{\mathrm{gw}} - \rho_{\infty}^{\mathrm{gw}}) + q^{\mathrm{gw}} + q^{\mathrm{w}} \quad \text{on } \Gamma_{\mathrm{c}}^{\mathrm{q}}, \tag{20b}$$

$$-(\rho^{\mathrm{w}}\mathbf{v}^{\mathrm{w}}\Delta h_{\mathrm{vap}} - \lambda_{\mathrm{eff}}\nabla T)\mathbf{n} = \alpha_{\mathrm{c}}(T - T_{\infty}) + q^{\mathrm{T}} \quad \text{on } \Gamma_{\mathrm{T}}^{\mathrm{q}} \quad \text{for } t \geqslant t_{\mathrm{o}}, \tag{20c}$$

where $\mathbf{n}$ is the unit vector, perpendicular to the surface of the porous medium, pointing towards the surrounding gas, $\rho_{\infty}^{\mathrm{gw}}$ and T_{∞} are respectively the mass concentration of water vapour and temperature in the undisturbed gas phase distant from the interface, α_{c} and β_{c} are convective heat and mass transfer coefficients respectively and q^{ga}, q^{gw}, q^{w} and q^{T} are the imposed dry air flux, imposed vapour flux, imposed liquid flux and imposed heat flux respectively.

 © 1998 John Wiley & Sons, Ltd.

The traction boundary conditions for the displacement field are

$$\boldsymbol{\sigma}\mathbf{n} = \hat{\mathbf{t}} \quad \text{on } \Gamma_{\mathrm{u}}^{\mathrm{q}} \quad \text{for } t \geqslant t_{\mathrm{o}}, \tag{21}$$

where $\hat{\mathbf{t}}$ is the imposed traction.

3. ISOTHERMAL TWO-PHASE FLOW APPROACH TO CAVITATION SIMULATION

As in Reference 3, we consider undrained situations, where cavitation has been experimentally observed.[1] In such conditions, with the exception of air bubbles in the water, which may be present in fully saturated specimens at low pressures, only two fluid phases are present after desaturation due to cavitation: liquid water and water vapour. An isothermal two-phase flow approach is adopted here; hence the air mass balance equation (14) and the energy balance equation (16) are not needed, because we assume that no air is present in the pores of the medium and that the temperature is constant.

An isothermal approach means physically that heat is supplied or taken away at infinite rate to maintain constant temperature (hence this implies infinite heat capacity value); thus there are no energetic restrictions on phase change (evaporation or condensation).

Thus finally our isothermal model consists of the linear momentum balance equation for the multiphase medium, (12), and the mass balance equation for the water species (15), with the diffusion term omitted (there is no diffusion of the water vapour in the air). Actually the Clausius–Clapeyron equation is not needed in Kelvin's law (5), because the water saturation pressure p^{gws} is constant in isothermal conditions.

From the assumption about absence of air in the pores of the medium it follows that the average pressure (7) is given by the relation

$$p = S_{\mathrm{w}} p^{\mathrm{w}} + S_{\mathrm{g}} p^{\mathrm{gw}} - p_{\mathrm{atm}}. \tag{22}$$

In the linear momentum balance equations for the multiphase medium, (12), and the fluids, (15), we ignore the relative component of the fluid accelerations. This allows us to reduce the primary variables to solid displacements and fluid pressure.[14] After introduction of the effective stress (6) into the linear momentum balance equation (12), we obtain its final form as

$$\operatorname{div}[\boldsymbol{\sigma}'' - \bar{\alpha}(S_{\mathrm{w}} p^{\mathrm{w}} + S_{\mathrm{g}} p^{\mathrm{gw}} - p_{\mathrm{atm}})\mathbf{I}] + \rho(\mathbf{g} - \mathbf{a}^{\mathrm{s}}) = 0. \tag{23}$$

The dynamic seepage forcing term in (15), connected with the solid acceleration, is very small when compared with other terms of the equation system, so it is neglected.[4] In isothermal conditions, at temperature $T = T_{\mathrm{o}}$, the vapour pressure depends only on the water pressure value:

$$p^{\mathrm{gw}} = p^{\mathrm{gws}}(T_{\mathrm{o}}) \exp\left(-\frac{(p^{\mathrm{gw}} - p^{\mathrm{w}})M_{\mathrm{w}}}{\rho^{\mathrm{w}} R T_{\mathrm{o}}}\right); \tag{24}$$

hence the water vapour gradient appearing in (15) can be expressed as

$$\operatorname{grad} p^{\mathrm{gw}} = \frac{\partial p^{\mathrm{gw}}}{\partial p^{\mathrm{w}}} \operatorname{grad} p^{\mathrm{w}}. \tag{25}$$

The capillary pressure in (24) has been eliminated using (2), which, because of the absence of air in the pores of the medium, reads

$$p^{\mathrm{c}} = p^{\mathrm{gw}} - p^{\mathrm{w}}. \tag{26}$$

© 1998 John Wiley & Sons, Ltd.

Introduction of (25) allows the balance equation for the water species (both liquid water and water vapour) in the partially saturated regime to be written as

$$\frac{\partial}{\partial t}[n(S_w\rho^w + S_g\rho^{gw})] + (S_w\rho^w + S_g\rho^{gw})\,\mathrm{div}\,\mathbf{v}^s - \mathrm{div}\left(\rho^w\frac{\mathbf{k}k^{rw}}{\mu^w}[\mathrm{grad}\,p^w - \rho^w(\mathbf{g}-\mathbf{a}^s)] + \rho^{gw}\frac{\mathbf{k}k^{rg}}{\mu^g}\frac{\partial p^{gw}}{\partial p^w}\,\mathrm{grad}\,p^w\right) = 0. \tag{27}$$

The terms in (23) and (27) related to the pressure and density of the water vapour will be obtained by use of the Kelvin equation (24) and the Clapeyron equation (3).

Together with equations (3), (23), (24) and (27) we need the constitutive equations of the medium, i.e.

$$S_w = S_w(p^c), \qquad k^{rw} = k^{rw}(S_w), \qquad k^{rg} = k^{rg}(S_w), \tag{28}$$

and the appropriate initial and boundary conditions (18) and (20b).

Cavitation may occur if the absolute pressure of the water is equal to or smaller than the saturation water vapour pressure at the temperature of the surrounding water (neglecting the surface tension on the interface of the arising vapour bubbles). Thus for the thermodynamic equilibrium state (assumed during formulation of the model) the vapour pressure on the interface between saturated and partially saturated porous material ($p^c = 0$) is equal to the saturation value, e.g. at $T = 20\,^\circ\mathrm{C}$, $p^{gws} = 2339$ Pa.

Note that the final form of our equations (23) and (27) is similar to the governing equations of the fully saturated state model,[16] even with the same two state variables: water pressure p^w and displacement vector $\mathbf{u}$; we have, however, to obtain the vapour pressure from (24).

Equation (24), having an implicit form, will be calculated iteratively, simultaneously with the main iterations of a Newton–Raphson type solution procedure, using in the RHS of (24) the value of p^{gw} from the previous iteration. The differences between the values of water vapour pressure at two successive iterations are very small because of the very low value of the term $\partial p^{gw}/\partial p^w$ (see next section); thus the method applied has sufficient accuracy.

4. DISCRETIZATION AND SOLUTION

The governing equations are discretized in space using finite elements and in the time domain by means of Newmark's scheme.[17] The unknown field variables are expressed in the whole domain by global shape function matrices $\mathbf{N}_u$ and $\mathbf{N}_w$ and nodal value vectors $\bar{\mathbf{u}}$ and $\bar{\mathbf{p}}$:

$$\mathbf{u} = \mathbf{N}_u\bar{\mathbf{u}}, \qquad \mathbf{p}^w = \mathbf{N}_w\bar{\mathbf{p}}. \tag{29}$$

A weak form of the linear momentum balance equation (23) and the mass balance equation (26), obtained following a Galerkin procedure,[17] can be expressed in matrix form as

$$\mathbf{M}\ddot{\bar{\mathbf{u}}} + \bar{\mathbf{P}} - \mathbf{Q}^w\bar{\mathbf{p}} = \mathbf{f}^u, \tag{30}$$

$$(\mathbf{H}^w + \mathbf{H}^v)\bar{\mathbf{p}} + (\mathbf{Q}^w + \mathbf{Q}^v)^T\dot{\bar{\mathbf{u}}} + (\mathbf{S}^w + \mathbf{S}^v)\dot{\bar{\mathbf{p}}} = \mathbf{f}^p, \tag{31}$$

where the equivalent nodal force vector $\bar{\mathbf{P}}$, the mass matrix $\mathbf{M}$, the coupling matrices $\mathbf{Q}^\pi$, the permeability matrices $\mathbf{H}^\pi$, the compressibility matrices $\mathbf{S}^\pi$, the external load vector $\mathbf{f}^u$, and the flow vector $\mathbf{f}^p$ are as defined in Appendix I. The superscripts 'w' and 'v' refer to water and vapour respectively.

 © 1998 John Wiley & Sons, Ltd.

Thus the coupled equation system at time level t_{n+1} can be written in the form

$$\begin{aligned}&\mathbf{M}_{n+1}\ddot{\bar{\mathbf{u}}}_{n+1}+\bar{\mathbf{P}}_{n+1}-\mathbf{Q}^{\mathrm{w}}_{n+1}\bar{\mathbf{p}}_{n+1}=\mathbf{f}^{\mathrm{u}}_{n+1},\\&(\mathbf{Q}^{\mathrm{w}}_{n+1}+\mathbf{Q}^{\mathrm{v}}_{n+1})^{\mathrm{T}}\dot{\bar{\mathbf{u}}}_{n+1}+(\mathbf{H}^{\mathrm{w}}_{n+1}+\mathbf{H}^{\mathrm{v}}_{n+1})\bar{\mathbf{p}}_{n+1}+(\mathbf{S}^{\mathrm{w}}_{n+1}+\mathbf{S}^{\mathrm{v}}_{n+1})\dot{\bar{\mathbf{p}}}_{n+1}=\mathbf{f}^{\mathrm{p}}_{n+1}.\end{aligned}\tag{32}$$

The Newmark scheme adopted for time integration, with the lowest allowable order for each variable, permits us to write the variables and their derivatives at time level t_{n+1} as a function of their values at the previous time level t_n and the increments of unknown variables between t_n and t_{n+1}:

$$\begin{aligned}\dot{\bar{\mathbf{u}}}_{n+1}&=\dot{\bar{\mathbf{u}}}_n+\ddot{\bar{\mathbf{u}}}_n\Delta t+\beta_1\Delta\ddot{\bar{\mathbf{u}}}_n\Delta t=\ddot{\bar{\mathbf{u}}}^{\mathrm{p}}_{n+1}+\beta_1\Delta\dot{\bar{\mathbf{u}}}_n\Delta t,\\\bar{\mathbf{u}}_{n+1}&=\bar{\mathbf{u}}_n+\dot{\bar{\mathbf{u}}}_n\Delta t+\frac{\ddot{\bar{\mathbf{u}}}_n\Delta t^2}{2}+\beta_2\Delta\ddot{\bar{\mathbf{u}}}_n\Delta t^2=\dot{\bar{\mathbf{u}}}^{\mathrm{p}}_{n+1}+\beta_2\Delta\ddot{\bar{\mathbf{u}}}_n\Delta t^2,\\\bar{\mathbf{p}}_{n+1}&=\bar{\mathbf{p}}_n+\dot{\bar{\mathbf{p}}}_n\Delta t+\Theta\Delta\dot{\bar{\mathbf{p}}}_n\Delta t=\bar{\mathbf{p}}^{\mathrm{p}}_{n+1}+\Theta\Delta\dot{\bar{\mathbf{p}}}_n\Delta t,\end{aligned}\tag{33}$$

where $\dot{\bar{\mathbf{u}}}^{\mathrm{p}}_{n+1}$, $\bar{\mathbf{u}}^{\mathrm{p}}_{n+1}$ and $\bar{\mathbf{p}}^{\mathrm{p}}_{n+1}$ are predicted values from known parameters at time level t_n and β_1, β_2 and Θ are the Newmark parameters.

Insertion of equations (33) into (32) allows the equation system to be written as

$$\begin{aligned}&\boldsymbol{\Psi}^{\mathrm{u}}_{n+1}=\mathbf{M}_{n+1}\Delta\ddot{\bar{\mathbf{u}}}_n+\bar{\mathbf{P}}_{n+1}-\mathbf{Q}^{\mathrm{w}}_{n+1}\Theta\Delta t\Delta\dot{\bar{\mathbf{p}}}_n-\mathbf{F}^{\mathrm{u}}_{n+1}=0,\\&\boldsymbol{\Psi}^{\mathrm{p}}_{n+1}=(\mathbf{Q}^{\mathrm{w}}_{n+1}+\mathbf{Q}^{\mathrm{v}}_{n+1})^{\mathrm{T}}\beta_1\Delta t\Delta\ddot{\bar{\mathbf{u}}}_n+(\mathbf{H}^{\mathrm{w}}_{n+1}+\mathbf{H}^{\mathrm{v}}_{n+1})\Theta\Delta t\Delta\dot{\bar{\mathbf{p}}}_n+(\mathbf{S}^{\mathrm{w}}_{n+1}+\mathbf{S}^{\mathrm{v}}_{n+1})\Delta\dot{\bar{\mathbf{p}}}_n-\mathbf{F}^{\mathrm{p}}_{n+1}=0,\end{aligned}\tag{34}$$

where the vectors $\mathbf{F}^{\mathrm{u}}_{n+1}$, and $\mathbf{F}^{\mathrm{p}}_{n+1}$ are as defined in Appendix I. At the beginning of each time step $\bar{\mathbf{P}}_{n+1}$ must be evaluated by integration of the rate elastoplastic constitutive law, knowing the stress field at the previous step. Also the vapour pressure and density must be evaluated from (24) and (3), respectively.

The coupled equation system (34) is non-linear because of the constitutive laws for the solid skeleton and for the capillary pressure and saturation. It is hence linearized by an iterative Newton–Raphson-type procedure

$$\boldsymbol{\Psi}^{\pi}_i+\left.\frac{\partial\boldsymbol{\Psi}^{\pi}_i}{\partial x}\right|_{x=x_i}\Delta x_i=0,\tag{35}$$

where the Jacobian matrix of transformation, $\mathbf{J}$, at the ith iteration is

$$\mathbf{J}=\left.\frac{\partial\boldsymbol{\Psi}}{\partial x}\right|_{x=x_i}=\begin{pmatrix}\dfrac{\partial\boldsymbol{\Psi}^{\mathrm{u}}}{\partial(\Delta\ddot{\bar{\mathbf{u}}})} & \dfrac{\partial\boldsymbol{\Psi}^{\mathrm{u}}}{\partial(\Delta\dot{\bar{\mathbf{p}}})}\\[2ex]\dfrac{\partial\boldsymbol{\Psi}^{\mathrm{p}}}{\partial(\Delta\ddot{\bar{\mathbf{u}}})} & \dfrac{\partial\boldsymbol{\Psi}^{\mathrm{p}}}{\partial(\Delta\dot{\bar{\mathbf{p}}})}\end{pmatrix}=\begin{pmatrix}\mathbf{M}+\mathbf{K}_{\mathrm{T}}\beta_2\Delta t^2 & -\mathbf{Q}^{\mathrm{w}}\Theta\Delta t\\(\mathbf{Q}^{\mathrm{w}}+\mathbf{Q}^{\mathrm{v}})^{\mathrm{T}}\beta_1\Delta t & (\mathbf{H}^{\mathrm{w}}+\mathbf{H}^{\mathrm{v}})\Theta\Delta t+\mathbf{S}^{\mathrm{w}}+\mathbf{S}^{\mathrm{v}}\end{pmatrix}\tag{36}$$

and $\mathbf{K}_{\mathrm{T}}$ is the elastoplastic tangent stiffness matrix.

Substituting (36) in (35) and scalar multiplying the second set of equations by $-\Theta/\beta_1$, we obtain the following equation system to be solved:

$$\begin{pmatrix}\mathbf{M}+\mathbf{K}_{\mathrm{T}}\beta_2\Delta t^2 & -\mathbf{Q}^{\mathrm{w}}\Theta\Delta t\\-(\mathbf{Q}^{\mathrm{w}}+\mathbf{Q}^{\mathrm{v}})^{\mathrm{T}}\Theta\Delta t & -\dfrac{\Theta}{\beta_1}[(\mathbf{H}^{\mathrm{w}}+\mathbf{H}^{\mathrm{v}})\Theta\Delta t+\mathbf{S}^{\mathrm{w}}+\mathbf{S}^{\mathrm{v}}]\end{pmatrix}\begin{pmatrix}\Delta\ddot{\bar{\mathbf{u}}}\\\Delta\dot{\bar{\mathbf{p}}}\end{pmatrix}=\begin{pmatrix}-\boldsymbol{\Psi}^{\mathrm{u}}\\-\dfrac{\Theta}{\beta_1}\boldsymbol{\Psi}^{\mathrm{p}}\end{pmatrix}.\tag{37}$$

Note that the multiplication by $-\Theta/\beta_1$ has been carried out to maintain a formal similarity of equation (37) with that for the fully saturated state.[3,4,16] The system is, however, non-symmetric. It

© 1998 John Wiley & Sons, Ltd.

has been further symmetrized by transferring the coupling term related to the water vapour to the RHS of the second equation:

$$\begin{pmatrix} \mathbf{M}+\mathbf{K}_{\mathrm{T}}\beta_2\Delta t^2 & -\mathbf{Q}^{\mathrm{w}}\Theta\Delta t \\ -(\mathbf{Q}^{\mathrm{w}})^{\mathrm{T}}\Theta\Delta t & -\dfrac{\Theta}{\beta_1}[(\mathbf{H}^{\mathrm{w}}+\mathbf{H}^{\mathrm{v}})\Theta\Delta t+\mathbf{S}^{\mathrm{w}}+\mathbf{S}^{\mathrm{v}}] \end{pmatrix} \begin{pmatrix} \Delta\ddot{\mathbf{u}} \\ \Delta\dot{\mathbf{p}} \end{pmatrix} = \begin{pmatrix} -\boldsymbol{\Psi}^{\mathrm{u}} \\ -\dfrac{\Theta}{\beta_1}\boldsymbol{\Psi}^{\mathrm{p}}+(\mathbf{Q}^{\mathrm{v}})^{\mathrm{T}}\Delta\ddot{\mathbf{u}}\Theta\Delta t \end{pmatrix}. \quad (38)$$

During computations this coupling term has been evaluated using $\Delta\ddot{\mathbf{u}}$ from the previous iteration.

It should be underlined that this and other terms with the superscript 'v' in the second equation are very small in comparison with the water-related terms (superscript 'w'), because all of them contain the factor $\rho^{\mathrm{gw}}/\rho^{\mathrm{w}}$, e.g. at $T = 20\,^{\circ}\mathrm{C}$, $\rho^{\mathrm{gw}}/\rho^{\mathrm{w}} \approx \rho^{\mathrm{gws}}/\rho^{\mathrm{w}} = 0{\cdot}01731/998{\cdot}21 \approx 1{\cdot}73\times10^{-5}$.

A similar value is taken by the factor $\partial p^{\mathrm{gw}}/\partial p^{\mathrm{w}}$ factor present in many terms of (38), for which

$$\frac{\partial p^{\mathrm{gw}}}{\partial p^{\mathrm{w}}} = \left(\frac{p^{\mathrm{gw}}M_{\mathrm{w}}}{\rho_{\mathrm{w}}RT}\right)\left(1+\frac{p^{\mathrm{gw}}M_{\mathrm{w}}}{\rho_{\mathrm{w}}RT}\right)^{-1} = \frac{\rho^{\mathrm{gw}}}{\rho_{\mathrm{w}}}\left(1+\frac{\rho^{\mathrm{gw}}}{\rho_{\mathrm{w}}}\right)^{-1} \approx \frac{\rho^{\mathrm{gw}}}{\rho_{\mathrm{w}}}. \quad (39)$$

The Newton–Raphson method requires the Jacobian matrix to be evaluated and inverted at each iteration; thus Davidon's modified scheme using secant updates has been used, because it achieves convergence with less computational effort and was found advantageous in non-linear analyses of porous media.[4]

Numerical problems often arise during computations when a rapid desaturation process in the zone near the shear band front occurs. In fact, very fast water pressure changes occur computationally in this zone, such that the saturation falls rapidly from one to almost its minimum value (irreversible saturation level) during a very short period of time (e.g. about 0·001 s in the examples described in the next section). Because in the same region other physical and numerical instabilities are also present, usually serious problems with convergence arise. Extensive tests carried out have shown that the source of these problems is the term C_{s} (containing $\partial S_{\mathrm{w}}/\partial p^{\mathrm{w}}$) in the compressibility matrix $\mathbf{S}^{\mathrm{w}}$ (see Appendix I). Application of a smaller time step length usually does not improve the situation. However, an efficient way of avoiding the mentioned problems is multiplication of the term C_{s} by a 'weighting factor' smaller than one. Since the term C_{s} is of importance only in the region near the shear band front, the general picture of the whole phenomenon should not be changed too much because of this. It is recalled that this term is missing altogether in some models of unsaturated flow (see e.g. Reference 18) and its influence should not be too large. This term is, however, maintained in our model but with a reduced weight.

5. NUMERICAL EXAMPLE

As a numerical example we use the dynamic strain localization problem, which was previously solved for fully saturated soil by Loret and Prevost[19] and Schrefler *et al.*[16]. Then Schrefler *et al.*[3] observed numerically for the same problem, using a simplified one-phase flow model, the occurrence of cavitation for dilatant material with impervious boundaries. This is in accordance with experimental observations carried out by Mokni.[1] Here this example is further analysed, by means of a two-phase flow model, to evaluate the influence of the terms related to the water vapour and then to compare strain localization phenomena in two different materials: sand and loam.

The sample of fully saturated soil (plain strain) is shown in Figure 1. It has impervious boundaries. Vertical and horizontal displacements are constrained at the bottom surface. Ramp loading is applied at the top, as indicated in Figure 1. During computations the self-weights of the soil and the water filling its pores are taken into account. A hydrostatic distribution of water pressure is assumed as initial condition.

 © 1998 John Wiley & Sons, Ltd.

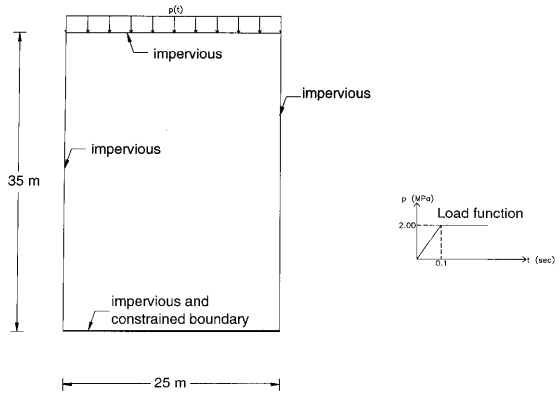

Figure 1. Scheme of analysed example

Two different materials are considered. For the first one, with an intrinsic permeability $k = 0{\cdot}55 \times 10^{-11}$ m^2, the relationships between capillary pressure, saturation and water relative permeability (Figures 2 and 3) proposed by Safai and Pinder[18] for San Fernando sand are used. In the partially saturated region the gas relative permeability–saturation relationship of Brooks and Corey[20] (with $\lambda = 3$) is applied (Figure 3). A Mohr–Coulomb yield criterion with associative flow rule and isotropic linear softening is used. The material parameters used during the computations are presented in Table I.

The second material analysed has an intrinsic permeability $k = 0{\cdot}55 \times 10^{-13}$ m^2 and the constitutive relationships of Safai and Pinder[18] for loam (Figure 2). Also for this material in the partially saturated region the gas relative permeability–saturation relationship of Brooks and Corey[20] (with $\lambda = 3$) is assumed (Figure 3). Other material parameters are the same as for the first case, except the apparent cohesion c_o which equals 2·0 MPa instead of 1·84 MPa.

Two different meshes of 396 (18 elements in width and 22 over the height) and 720 (24×30) four-node isoparametric finite elements (FEs) of equal size, the same for displacements and water

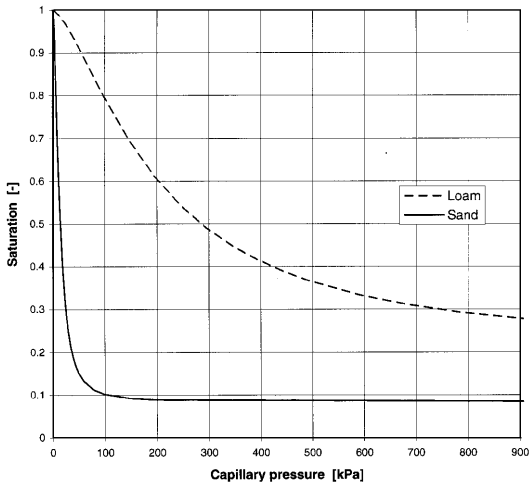

Figure 2. Constitutive relationship between capillary pressure and saturation for loam and San Fernando sand[18]

© 1998 John Wiley & Sons, Ltd.

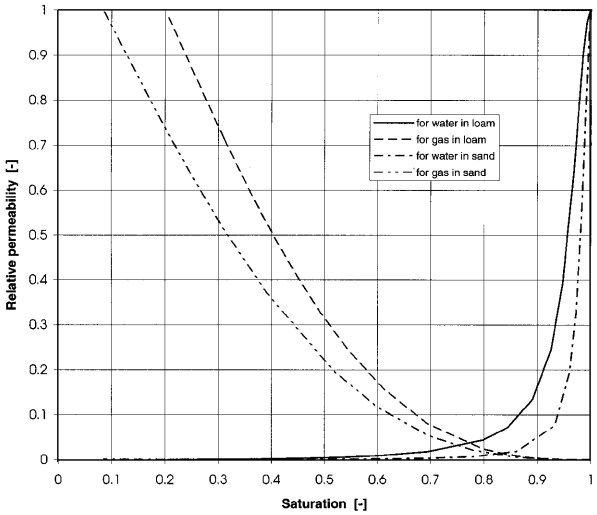

Figure 3. Relative permeabilities of water[18] and gas[20] in loam and San Fernando sand

pressures, have been used together with a one-point Gaussian integration scheme for the stiffness matrix. Computations are performed by use of the modified version of the Swandyne code,[4,5] with the initial time step length $\Delta t = 0{\cdot}001$ s in the elastic range, then reducing it 10–100 times depending on the case analysed. In all the examples solved the temperature is taken equal to 20 °C.

First the localization problem for the sand data (Table I) was solved, applying the present model and the previous simplified one,[3] where only one-phase flow was considered together with zero value of the relative water vapour pressure (with respect to atmospheric pressure). The results obtained with both approaches are compared to evaluate the practical significance of the terms related to the vapour. For both cases the weighting factor for the term C_s is equal to 0·001 and the same time step lengths ($\Delta t = 0{\cdot}001$ s in the elastic and $\Delta t = 0{\cdot}0001$ s in the plastic range) have been assumed. The computations have been performed for the mesh of 396 FEs.

The time histories of water pressure and vertical total strain at the same two points, inside and outside the shear band, are compared in Figures 4(a) and 4(b), showing that omitting the terms related to the gas phase results in smaller water pressures (higher capillary pressures) and larger absolute values of vertical total strain for points inside the shear band. The differences outside the band are less significant. The time value when the shear band is fully developed is about 0·01 s higher for the present model. The shape of the corresponding isolines for both water pressure, Figures 5 (a) and 5(b), and equivalent plastic strain, Figures 6(a) and 6(b) as well as for the other variables (e.g. capillary pressure, saturation, water flow rate), not shown here, is slightly different. Their minimal and maximal values for water pressure are changed: for the present model the maximal water

Table I

Young modulus	$E = 285$ MPa	Poisson ratio	$v = 0{\cdot}4285$
Solid grain density	$\rho^s = 2000$ kg m^{-3}	Liquid density	$\rho^w = 998{\cdot}2$ kg m^{-3}
Apparent cohesion	$c_o = 1{\cdot}84$ MPa	Hardening modulus	$H = -40$ MPa
Angle of internal friction	$\varphi = 20^\circ$	Initial porosity	$n = 0{\cdot}20$
Solid grain bulk modulus	$K_s = 6{\cdot}78$ GPa	Liquid phase bulk modulus	$K_w = 0{\cdot}20$ GPa
Gas phase bulk modulus	$K_g = 2{\cdot}34$ kPa	Biot constant	$\bar{\alpha} = 1{\cdot}0$

 © 1998 John Wiley & Sons, Ltd.

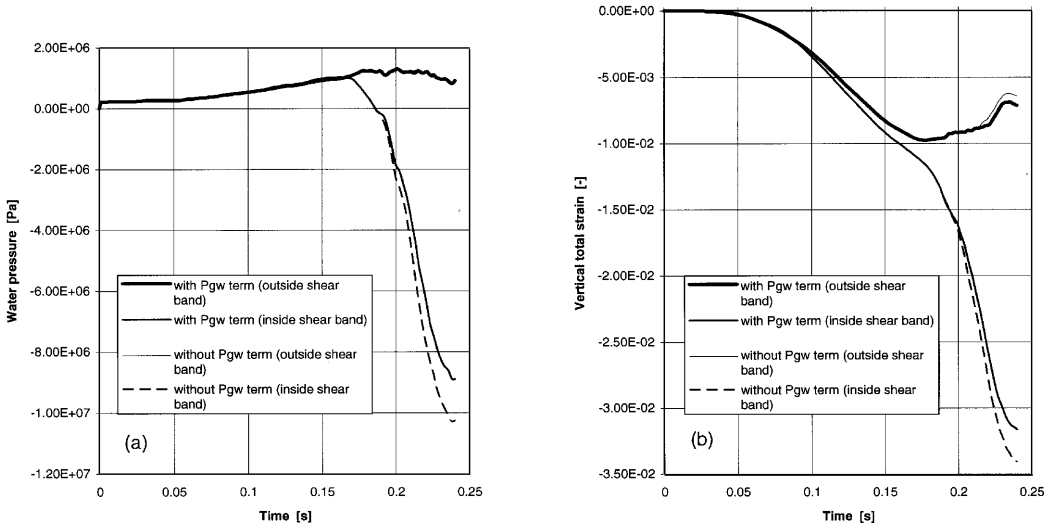

Figure 4. Comparison of two solutions for sand, obtained by use of present and previous[3] models, at same two points, inside and outside shear band: (a) water pressure history; (b) vertical total strain history

pressure is about 0·65 MPa higher and the minimal one about 3·4 MPa higher. Further, the maximal flow rate is about 0·0075 $\mathrm{m\,s^{-1}}$ lower. It should be underlined that the differences in the water pressure distribution are not caused by a simple addition of the constant pressure value $-(p^{\mathrm{gw}} - p_{\mathrm{atm}}) \approx 0{\cdot}1$ MPa, which was omitted in the previous model.[3] Hence the terms related to the water vapour, and omitted in Reference 3, are of importance for the full description of the phenomenon and should be taken into account during simulations: the more correct model is only slightly more complicated than the simplified one.

Finally the problem has been solved for sand and loam to show the combined effect of the material parameters and different constitutive capillary pressure–water degree of saturation relationship on the shear band development. In this case a mesh of 720 FEs has been applied. For both materials the same weighting factor for the term C_{s}, equal to 0·001, as well as the same time step length ($\Delta t = 0{\cdot}0001$ s in the plastic range) have been assumed.

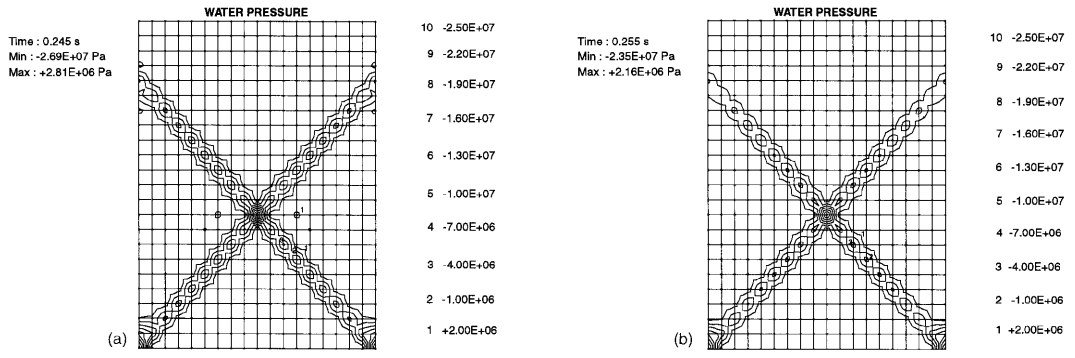

Figure 5. Comparison of water pressure fields in sand: (a) previous simplified model;[3] (b) present two-phase flow model

© 1998 John Wiley & Sons, Ltd.

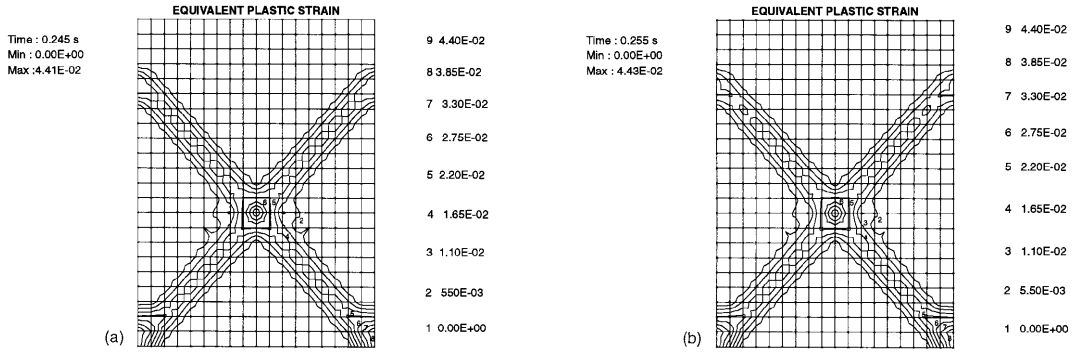

Figure 6. Comparison of equivalent plastic strain fields in sand: (a) previous simplified model;[3] (b) present two-phase flow model

The resulting isolines for water pressure, capillary pressure and equivalent plastic strain, as well as the flow rate graphs are presented in Figures 7(a)–7(d) for the sand and in Figures 8(a)–8(d) for the loam. The resulting time histories of water pressure and vertical total strain for the same two points, inside and outside the shear band, have been compared in Figures 9(a) and 9(b). In this case the differences are significant. The shear band in the loam is fully developed after a period of time twice as long as for the sand (about 0·21 s later) and for slightly higher absolute values of the equivalent

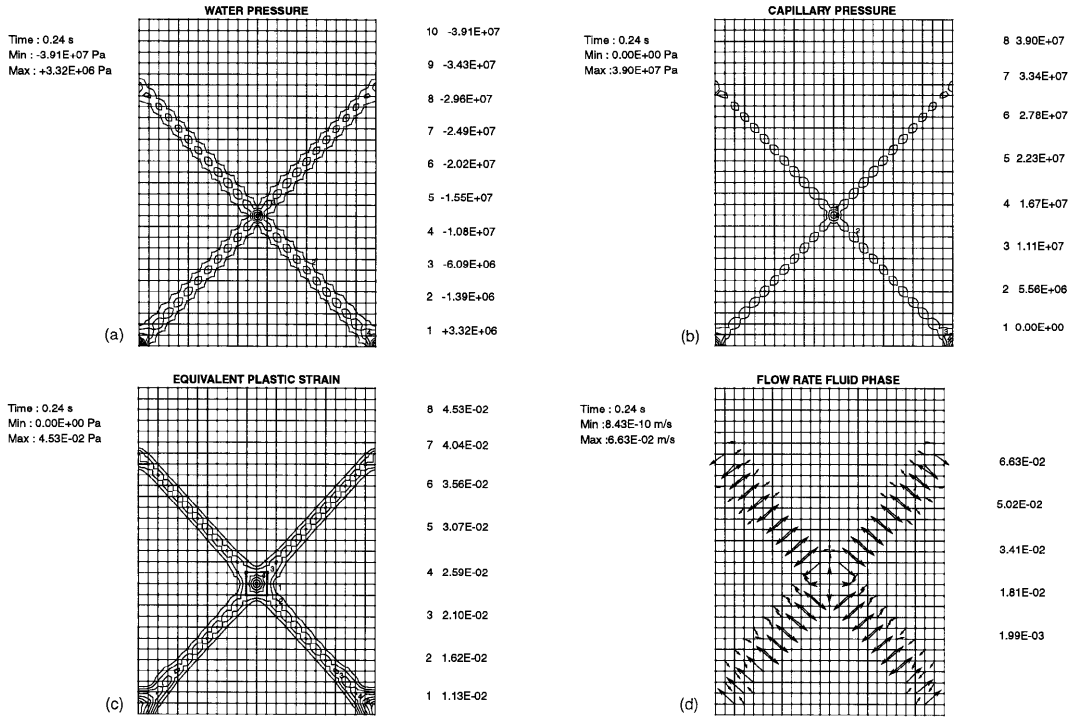

Figure 7. Results of computations for sand: (a) water pressure field; (b) capillary pressure field; (c) equivalent plastic strain field; (d) water flow rate field

 © 1998 John Wiley & Sons, Ltd.

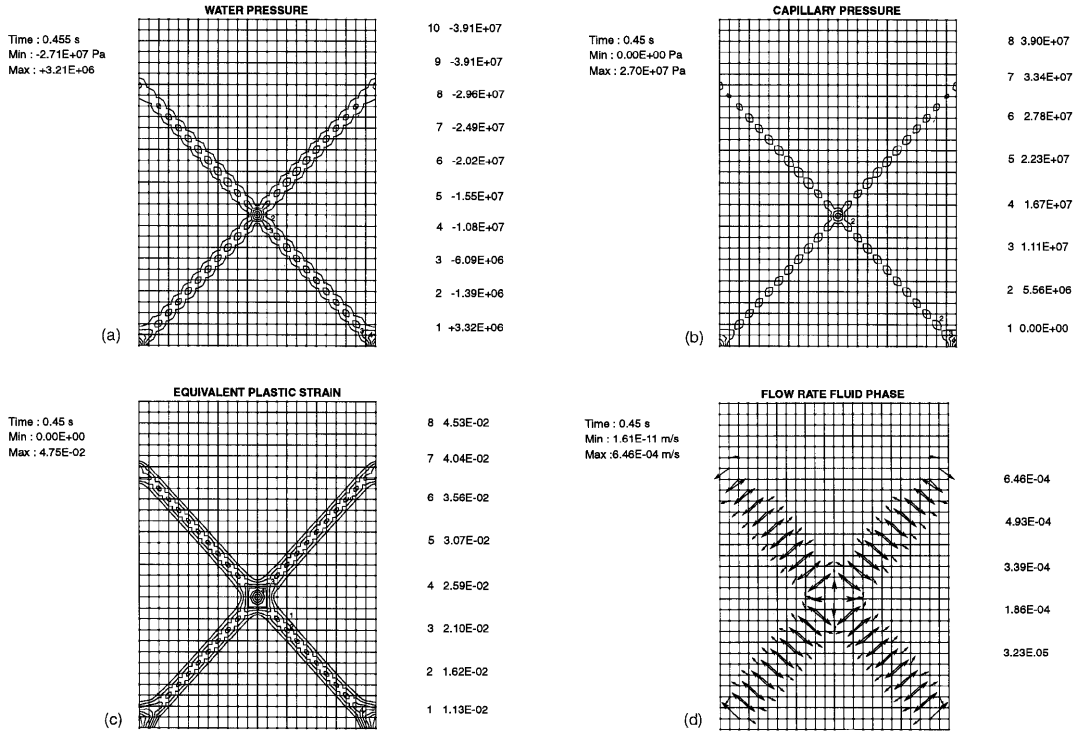

Figure 8. Results of computations for loam: (a) water pressure field; (b) capillary pressure field; (c) equivalent plastic strain field; (d) the water flow rate field

plastic strain because of the smaller intrinsic permeability and greater apparent cohesion value for the loam. The sand is more desaturated and in a slightly greater region than the loam, reaching higher values of capillary pressure (maximal value higher by about 12 MPa), while the maximal water pressure value in the loam is about 0·11 MPa lower. The water flow rates in the loam, because of the much smaller intrinsic permeability, are very distinctly lower: the maximal value about 100 times so.

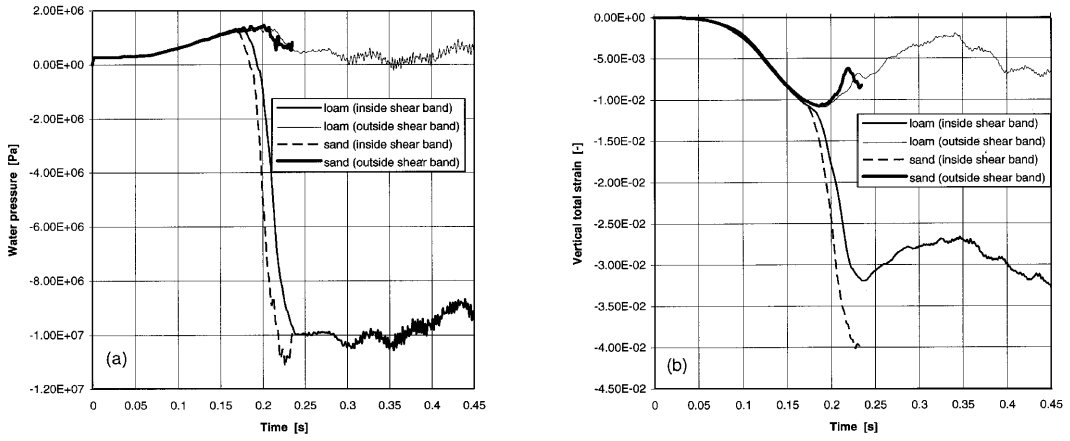

Figure 9. Comparison of results for sand and loam at same two points, inside and outside shear band: (a) water pressure history; (b) the vertical total strain history

© 1998 John Wiley & Sons, Ltd.

For both materials the vapour pressures in the desaturated regions of the shear band are practically constant (negligible gradient) and only slightly different from the saturation value (2339 Pa). The minimal vapour pressures at the point of the band crossing are 1949 Pa in the sand and 1973 Pa in the loam. As a consequence, the vapour flow rates in the desaturated zone are very small, about 1000 times lower than the water flow rates in the same region.

6. CONCLUSIONS

An isothermal two-phase flow model for the simulation of cavitation phenomena in partially saturated porous media has been presented. As compared with a previous simplified model, it requires the solution of the Kelvin equation in the form of a non-linear implicit equation for the vapour pressure and of the mass balance equation for the vapour. This second equation allows us to eliminate the mass rate of evaporation from the mass balance equation of the water phase. Also the effective stress principle is modified to take into account two-phase flow. These modifications have been introduced in the Swandyne[4,5] finite element code for soil dynamics and problems relating to dynamic strain localization in samples of dense sand have been solved. It has been shown that the previously neglected terms relating to the water vapour are of importance and should be taken into account in a more correct simulation of the phenomena.

ACKNOWLEDGEMENTS

This work has been carried out within the framework of HCM project 'ALERT geomaterials' and was partly financed by the Italian Ministry of Scientific and Technological Research (MURST 40%).

APPENDIX I: DEFINITIONS OF VECTORS AND MATRICES

$$\mathbf{M} = \int_\Omega \mathbf{N}_\mathrm{u}^\mathrm{T}[\rho^\mathrm{s}(1-n) + \rho^\mathrm{w} n S_\mathrm{w}]\mathrm{N}_\mathrm{u}\, \mathrm{d}\Omega,$$

$$\bar{\mathbf{P}} = \int_\Omega \mathbf{B}^\mathrm{T}\boldsymbol{\sigma}''\, \mathrm{d}\Omega,$$

$$\mathbf{Q}^\mathrm{w} = -\int_\Omega \mathbf{B}^\mathrm{T}\bar{\alpha} S_\mathrm{w}\, \mathbf{m}\mathbf{N}_\mathrm{w}\, \mathrm{d}\Omega, \quad \text{where } \mathbf{m} = (1, 1, 1, 0, 0, 0)^\mathrm{T},$$

$$\mathbf{Q}^\mathrm{v} = -\int_\Omega \mathbf{B}^\mathrm{T} \frac{\rho^\mathrm{gw}}{\rho^\mathrm{w}} \bar{\alpha} S_\mathrm{g} \mathbf{m}\mathbf{N}_\mathrm{w}\, \mathrm{d}\Omega,$$

$$\mathbf{f}^\mathrm{u} = \int_\Omega \mathbf{N}_\mathrm{u}^\mathrm{T}[\rho^\mathrm{s}(1-n) + \rho^\mathrm{w} n S_\mathrm{w}]\mathbf{g}\, \mathrm{d}\Omega + \int_\Gamma \mathbf{N}_\mathrm{u}^\mathrm{T}\mathbf{t}\, \mathrm{d}\Gamma + \int_\Omega \mathbf{B}^\mathrm{T}\bar{\alpha}(S_\mathrm{g} p^\mathrm{gw} - p_\mathrm{atm})\mathbf{m}\mathbf{N}_\mathrm{w}\, \mathrm{d}\Omega.$$

$$\mathbf{f}^\mathrm{p} = \int_\Omega (\nabla \mathbf{N}_\mathrm{w})^\mathrm{T}\mathbf{k}\rho^\mathrm{w}\mathbf{g}\, \mathrm{d}\Omega - \int_{\Gamma_\mathrm{w}} \mathbf{N}_\mathrm{p}^\mathrm{T}\mathbf{q}^\mathrm{T}\mathbf{n}\, \mathrm{d}\Gamma,$$

 © 1998 John Wiley & Sons, Ltd.

$$\mathbf{H}^{\mathrm{w}} = -\int_{\Omega} (\nabla \mathbf{N}_{\mathrm{w}})^{\mathrm{T}} k_{\mathrm{w}} \nabla \mathbf{N}_{\mathrm{w}} \, \mathrm{d}\Omega,$$

$$\mathbf{H}^{\mathrm{v}} = -\int_{\Omega} (\nabla \mathbf{N}_{\mathrm{w}})^{\mathrm{T}} k_{\mathrm{g}} \frac{\rho^{\mathrm{gw}}}{\rho^{\mathrm{w}}} \frac{\partial p^{\mathrm{gw}}}{\partial p^{\mathrm{w}}} \nabla \mathbf{N}_{\mathrm{w}} \, \mathrm{d}\Omega,$$

$$\mathbf{S}^{\mathrm{w}} = \int_{\Omega} \mathbf{N}_{\mathrm{w}}^{\mathrm{T}} \frac{1}{Q_{\mathrm{w}}} \mathbf{N}_{\mathrm{w}} \, \mathrm{d}\Omega,$$

$$\mathbf{S}^{\mathrm{v}} = \int_{\Omega} \mathbf{N}_{\mathrm{w}}^{\mathrm{T}} \frac{\rho^{\mathrm{gw}}}{\rho^{\mathrm{w}}} \frac{1}{Q_{\mathrm{v}}} \mathbf{N}_{\mathrm{w}} \, \mathrm{d}\Omega,$$

$$\mathbf{F}^{\mathrm{u}}_{n+1} = \mathbf{f}^{\mathrm{u}}_{n+1} - \mathbf{M}_{n+1} \ddot{\bar{\mathbf{u}}}_n + \mathbf{Q}^{\mathrm{w}}_{n+1} (\bar{\mathbf{p}}_n + \Delta t \dot{\bar{\mathbf{p}}}_n),$$

$$\mathbf{F}^{\mathrm{p}}_{n+1} = \mathbf{f}^{\mathrm{p}}_{n+1} - (\mathbf{Q}^{\mathrm{w}}_{n+1} + \mathbf{Q}^{\mathrm{v}}_{n+1})^{\mathrm{T}} (\dot{\bar{\mathbf{u}}}_n + \Delta t \ddot{\bar{\mathbf{u}}}_n) - (\mathbf{H}^{\mathrm{w}}_{n+1} + \mathbf{H}^{\mathrm{v}}_{n+1})(\bar{\mathbf{p}}_n + \Delta t \, \Delta \dot{\bar{\mathbf{p}}}_n) - (\mathbf{S}^{\mathrm{w}}_{n+1} + \mathbf{S}^{\mathrm{v}}_{n+1}) \dot{\bar{\mathbf{p}}}_n,$$

$$\frac{1}{Q_{\mathrm{w}}} = C_{\mathrm{s}} + \frac{n S_{\mathrm{w}}}{K_{\mathrm{w}}} + \frac{\bar{\alpha} - n}{K_{\mathrm{s}}} S_{\mathrm{w}}^2 \left(1 + \frac{C_{\mathrm{s}}}{n S_{\mathrm{w}}} p^{\mathrm{w}} + \frac{S_{\mathrm{g}}}{S_{\mathrm{w}}} \frac{\partial p^{\mathrm{gw}}}{\partial p^{\mathrm{w}}} \right), \quad \text{where } C_{\mathrm{s}} = n \frac{\partial S_{\mathrm{w}}}{\partial p^{\mathrm{w}}},$$

$$\frac{1}{Q_{\mathrm{w}}} = -C_{\mathrm{s}} + \frac{n S_{\mathrm{g}}}{K_{\mathrm{g}}} + \frac{\partial p^{\mathrm{gw}}}{\partial p^{\mathrm{w}}} + \frac{\bar{\alpha} - n}{K_{\mathrm{s}}} S_{\mathrm{w}} S_{\mathrm{g}} \left(1 + \frac{C_{\mathrm{s}}}{n S_{\mathrm{w}}} p^{\mathrm{w}} + \frac{S_{\mathrm{g}}}{S_{\mathrm{w}}} \frac{\partial p^{\mathrm{gw}}}{\partial p^{\mathrm{w}}} \right).$$

APPENDIX II: NOMENCLATURE

s	solid phase
g	gaseous phase
gw	gaseous water phase, water vapour
w	liquid phase, water
π	generic phase
$\mathbf{a}^{\pi}$	acceleration of π-phase
$\mathbf{a}^{\pi \mathrm{s}}$	acceleration relative to solid
$\mathbf{B}$	linear strain operator
C_{s}	specific moisture capacity
$\mathbf{C}_{\mathrm{T}}$	tangential constitutive tensor
$\mathbf{D}_{\mathrm{g}}$	effective diffusivity tensor
$\mathbf{f}^{\mathrm{p}}$	flow load vector
$\mathbf{f}^{\mathrm{u}}$	external load vector
$\mathbf{g}$	gravity acceleration
$\mathbf{H}^{\pi}$	permeability matrix
$\mathbf{I}$	unit second-order tensor
$k^{\mathrm{r}\pi}$	liquid phase relative permeability
$\mathbf{k}$	absolute or intrinsic permeability tensor
$k = \mathbf{k} k^{\mathrm{r}\pi} \rho^{\mathrm{w}} \mathbf{g} / \mu$	permeability value ($\mathrm{m\,s^{-1}}$)
K_{s}	solid grain bulk modulus
K_{w}	liquid phase bulk modulus
$\mathbf{K}_{\mathrm{T}}$	elastoplastic tangential stiffness matrix
M_{π}	molar mass of constituent π

© 1998 John Wiley & Sons, Ltd.

$\mathbf{M}$	mass matrix
n	porosity
$\mathbf{n}$	unit normal vector
p^{π}	macroscopic pressure of π-phase
$\bar{\mathbf{P}}$	equivalent force vector
$\mathbf{Q}^{\pi}$	coupled matrix
R	universal constant gas
S_{w}	water saturation
S_{g}	gas saturation
$\mathbf{S}^{\pi}$	compressibility matrix
t	time variable
$\mathbf{t}$	surface traction tensor
T	temperature
$\mathbf{u}$	solid displacements
$\mathbf{v}^{\alpha\pi}$	velocity of α-phase with respect to π-phase
$\mathbf{v}^{\pi}$	velocity of π-phase
$\bar{\alpha}$	Biot coefficient
β_1, β_2, Θ	Newmark parameters
λ_{eff}	effective thermal conductivity
μ	liquid dynamic viscosity
ρ	porous medium density
ρ^{π}	intrinsic phase-averaged density of π-phase
$\boldsymbol{\sigma}$	Cauchy stress tensor
$\boldsymbol{\sigma}''$	effective stress tensor

Variables with overbar refers to the nodal values.

REFERENCES

1. M. Mokni, 'Relations entre déformations en masse et déformations localisées dans les matériaux granulaires', *Ph.D. Thesis*, Institut de Mécanique de Grenoble, 1992.
2. F. B. Damjanic and J. Radnic, 'Seismic analysis of fluid–structure interaction including cavitation', in B. A. Schrefler and O. C. Zienkiewicz (eds), *Computer Modelling in Ocean Engineering*, Balkema, Rotterdam, 1988, pp. 523–530.
3. B. A. Schrefler, L. Sanavia and C. E. Majorana, 'A multiphase medium model for localisation and postlocalisation simulation in geomaterials', *Mech. Cohes.–Frict. Mater*. in press.
4. Y. M. Xie, 'Finite element solution and adaptive analysis for static and dynamic problems of saturated–unsaturated porous media', *Ph.D. Thesis C/Ph/136/90*, Department of Civil Engineering, Swansea University, 1990.
5. E. A. Meroi, B. A. Schrefler and O. C. Zienkiewicz, 'Large strain static and dynamic semisaturated soil behaviour', *Int. j. num. anal. methods geomech*., **19**, 81–106 (1995).
6. B. A. Schrefler, 'F.E. in environmental engineering: coupled thermo–hydro–mechanical processes in porous media including pollutant transport', *Arch. Comput. Methods Eng*., **2**, 1–54 (1995).
7. M. Hassanizadeh and W. G. Gray, 'General conservation equations for multi-phase system: 1. Averaging technique', *Adv. Water Res*., **2**, 131–144 (1979).
8. M. Hassanizadeh and W. G. Gray, 'General conservation equations for multi-phase system: 2. Mass, momenta, energy and entropy equations', *Adv. Water Res*., **2**, 191–201 (1979).
9. M. Hassanizadeh and W. G. Gray, 'General conservation equations for multi-phase system: 3. Constitutive theory for porous media flow', *Adv. Water Res*., **3**, 25–40 (1980).
10. W. G. Gray and M. Hassanizadeh, 'Unsaturated flow theory including interfacial phenomena', *Water Resource Res*., **27**, 1855–1863 (1991).
11. *ASHRAE Handbook, Fundamentals Volume*, ASHRAE, Atlanta, GA, 1993.
12. R. W. Lewis and B. A. Schrefler, *The Finite Element Method in the Static and Dynamic Deformation and Consolidation of Porous Media*, Wiley, Chichester, 1997.
13. D. Gawin, P. Baggio and B. A. Schrefler, 'Coupled heat, water and gas flow in deformable porous media', *Int. j. numer. methods fluids*, **20**, 969–987 (1995).

 © 1998 John Wiley & Sons, Ltd.

14. O. C. Zienkiewicz, A. H. C. Chan, M. Pastor, D. K. Paul and T. Shiomi, 'Static and dynamic behaviour of soils: a rational approach to quantitative solutions. I—Fully saturated problems', *Proc. R. Soc. Lond. A*, **429**, 285–309 (1990).
15. O. C. Zienkiewicz, Y. M. Xie, B. A. Schrefler, A. Ladesma and N. Bicanic, 'Static and dynamic behaviour of soils: a rational approach to quantitative solutions. II—Semi-saturated problems', *Proc. R. Soc. Lond. A*, **429**, 311–321 (1990),
16. B. A. Schrefler, C. E. Majorana and L. Sanavia, 'Shear band localization in saturated porous media', *Arch. Mech.*, **47**, 577–599 (1995).
17. O. C. Zienkiewicz and R. L. Taylor, *The Finite Element Method*, Vol. 2, McGraw-Hill, London, 1991.
18. N. M. Safai and G. F. Pinder, 'Vertical and horizontal land deformation in a desaturating porous medium', *Adv. Water Resources*, **2**, 19–25 (1979).
19. B. Loret and J. H. Prevost, 'Dynamic strain localisation in fluid-saturated porous media', *J. Eng. Mech.*, **11**, 907–922 (1991).
20. R. N. Brooks and A. T. Corey, 'Properties of porous media affecting fluid flow', *J. Irrig. Drain. Div. Am. Soc. Civil Eng.*, **92**(IR2), 61–68 (1966).

© 1998 John Wiley & Sons, Ltd.